

A Self Contour-based Rotation and Translation-Invariant Transformation for Point Clouds Recognition

Dongrui Liu, *Student Member, IEEE*, Chuanchuan Chen, *Student Member, IEEE*, Changqing Xu, Qi Cai, Lei Chu, *Member, IEEE*, and Robert Caiming Qiu, *Fellow, IEEE*

Abstract—Recently, several direct processing point cloud models have achieved state-of-the-art performances for classification and segmentation tasks. However, these methods lack rotation robustness, and their performances degrade severely under random rotations, failing to extend to real-world applications with varying orientations. To address this problem, we propose a method named Self Contour-based Transformation (SCT), which can be flexibly integrated into a variety of existing point cloud recognition models against arbitrary rotations without any extra modifications. The SCT provides efficient and mathematically proved rotation and translation invariance by introducing Rotation and Translation-Invariant Transformation. It linearly transforms Cartesian coordinates of points to the self contour-based rotation-invariant representations while maintaining the global geometric structure. Moreover, to enhance discriminative feature extraction, the Frame Alignment module is further introduced, aiming to capture contours and transform self contour-based frames to the intra-class frame. Extensive experimental results and mathematical analyses show that the proposed method outperforms the state-of-the-art approaches under arbitrary rotations without any rotation augmentation on standard benchmarks, including ModelNet40, ScanObjectNN and ShapeNet. Code is available at <https://github.com/shenqildir/ScorNet>.

Index Terms—3D point clouds, classification, segmentation, rotation and translation invariance, 3D recognition.

I. INTRODUCTION

THREE dimensional (3D) point clouds have attracted tremendous attention due to the requirement of modern applications, such as robotics and autonomous driving [1]. Point clouds are discrete and unstructured representations of continuous 3D space. Thanks to their simplicity and secure acquisition [2], point clouds have been widely studied in computer vision and computer graphics [3]. Due to irregularity and sparsity, traditional regular convolutional neural networks (CNNs) fail to transfer to handle point clouds directly.

To take advantage of the powerful standard CNNs, point clouds are transformed into voxel-grids [4], [5], mesh [6] and multi-view projections [7], suffering from quantization artifacts and memory burden. PointNet [8] is the pioneer to consume point clouds directly with deep neural networks. It extracts point-wise feature through shared Multilayer Perceptrons and adopts a symmetric function max pooling to get global features while pursuing permutation invariance. After that,

many similar methods emerge to various tasks, such as point cloud classification [9], [10], segmentation [11], detection [12], [13]. Although the advancement of computational resources and 3D sensors enable researchers to consume point clouds directly [14]–[16], those methods are highly vulnerable to the effects of random rotations. Unlike the synthetic and aligned dataset, orientations of raw point clouds generated by LiDAR sensors are typically unknown and dynamic. Efficient and precise classification and segmentation of point clouds against rotations are essential for real-world scenarios e.g., autonomous driving. Thus, we mainly consider how to improve rotation robustness of various existing point cloud processing models for classification and part segmentation in this work.

A straightforward way to overcome the issue is to apply tremendous rotation augmentation to improve the orientation robustness of models. However, the infinite 3D rotation group (SO3) makes it impossible to design such a network with high capacity to extract consistent shape awareness features against random rotations [17]. Besides, it is computationally expensive and suffers from arbitrary rotation perturbations without meeting strict rotation invariance. Alternatively, several schemes have been recently proposed for developing rotation-invariant architectures [18]–[22]. PRIN [18] utilizes spherical voxel convolution to capture robust features without ensuring strict rotation invariance. PPF-FoldNet [19] and ClusterNet [20] build local descriptors to replace the Cartesian coordinates of points with relative angles and distances, which is time-consuming. SRINet [21] encodes point clouds through a nonlinear mapping, inevitably impairing the neighboring geometries. As obtaining rotation-invariant representations is such an essential part of these methods, detailed analysis and comparisons are discussed in Section IV, by examining time complexity and measuring performances under the same conditions. From this, it is clear that those rotation-invariant transformation methods limit their performances and become a bottleneck.

To address the drawback, we design a **Rotation and Translation-Invariant Transformation (RTIT)** module, linearly transforming Cartesian coordinates of points to the self contour-based rotation and translation-invariant representations while preserving global geometric structure. The versatile RTIT module can be flexibly integrated into a variety of point cloud analysis networks to pursue strict rotation and translation invariance.

However, the rotation and translation-invariant representations provided by the RTIT module make neural networks more

All authors are with the School of Electronic Information and Electrical Engineering, Shanghai Jiao Tong University (email: drliu96@sjtu.edu.cn; cccchensir@sjtu.edu.cn; cqxu@sjtu.edu.cn; sipangyiyou@sjtu.edu.cn; leochu@sjtu.edu.cn; reqiu@sjtu.edu.cn).

challenging to extract discriminative features because the point set from each object is transformed from the unified Cartesian frame to self contour-based frame. To tackle this issue, we further introduce a **Frame Alignment (FA)** module to capture contours and transform its self contour-based frame to an intra-class frame. Moreover, FA adds an alignment loss minimizing the difference between the estimated frame transformation and the ground truth frame transformation, which benefits the entire model.

Overall, we demonstrate the effectiveness of Self Contour-based Transformation SCT on point cloud classification and part segmentation tasks under arbitrary rotations. Extensive experimental results and mathematical analyses show that our proposed method outperforms the state-of-the-art approaches under arbitrary rotations without any rotation augmentation on standard benchmarks, including ModelNet40, ScanObjectNN and ShapeNet. The consistent performances on synthetic and real-world datasets show the generalization and robustness of our model. We will release our code to facilitate the future works.

The key contributions of our work are summarized below:

- We compare and analyze existing rotation-invariant architectures, identifying rotation-invariant transformation methods inhibits their extension to real-world applications.
- We introduce a Rotation and Translation-Invariant Transformation to enhance the rotation and translation robustness of different point cloud processing techniques while avoiding suffering from quantization artifacts with low computational complexity.
- We propose a Frame Alignment module that enhances the feature extraction process with a frame transformation operation, which is proved to be beneficial for the optimization of the entire model.
- Extensive experimental results and mathematical analyses have been conducted on synthetic and real-world benchmark datasets for classification and part segmentation tasks. The experimental results demonstrate that our method surpasses the state-of-the-art approaches under arbitrary rotations.

II. RELATED WORK

A. Voxel-Based models.

To extend effective 2D convolution to 3D recognition, VoxNet [4] and ShapeNets [5] convert point clouds to volumetric representations and apply the standard 3D convolution. Even with modern GPUs, these techniques could only process low resolution voxel-grids (e.g. 32x32x32 in VoxNet [4]). Octree [23], Kd-Tree [14] based methods were proposed to avoid the convolution in empty space to reduce memory consumption. OctNet [23] makes a prominent contribution, being able to handle high-resolution up to 256x256x256. Along this direction, subsequent methods went on to process voxel and grids [24]–[29]. Meanwhile, many works projected point clouds onto 2D images for recognition [30]–[33]. Though these organized and efficient data structures save time complexity, the high memory cost and resolution loss are inevitable.

B. Point-Based models.

PointNet [8] is the pioneer to process the unordered point clouds directly with neural networks. It extracts point-wise features through shared Multilayer Perceptrons (MLPs) from the simply (x, y, z) coordinates, and adopts a symmetric function max pooling to get global features while pursuing permutation invariance. Since neglecting to mine neighbor relationship, various networks are proposed to remedy it. PointNet++ [9] uses PointNets to hierarchically capture local features and enhance the local interactions. ECC [34] analyzes neighboring points by spectral graph convolution and a graph pooling strategy. DGCNN [10] constructs dynamic local graphs and extracts semantic relation with EdgeConv operation. PointCNN [35] reorders the local points with a convolution operation named χ -Conv. SO-Net [36] utilizes a self-organizing map to establish neighbor interaction. Besides, some works were proposed for point convolution [37]–[39], kernel-based convolution [40]–[43], unsupervised learning [44]–[47]. However, most of them are vulnerable to random rotations, which are very general among real-world applications.

C. Rotation-Invariant models.

Thomas *et al.* [48] achieved local rotations equivalence by designing filters built from spherical harmonics and extending it to the tensor field neural networks. The researchers [49], [50] proposed a spherical convolution operation to learn rotation-invariant features from spherical representations. Similarly, PRIN employs Spherical Voxel Convolution to capture robust features. However, these spherical voxel convolution-based techniques do not guarantee strictly and globally rotation invariance and are sensitive to the noise. ClusterNet [20] builds K-nearest neighbor graphs and transforms Cartesian coordinates into relative angles and distances to harvest local rotation invariance. Then utilizing a clustering operation extracts features, which is time-consuming and not applicable to the segmentation task. SRINet [18] encodes point clouds through a nonlinear projection mapping, inevitably impairing the neighboring geometries. Detailed analysis and comparisons are discussed in Section IV. In contrast, our Contour-Aware Transformation adopts a global linear transformation, which is rigorously rotation and translation-invariant while maintaining the geometric structures.

III. METHOD

A. Method Overview

The original point clouds collected by 3D sensors or laser scanners usually contains many attributes, such as 3D coordinates, RGB colors, surface normal and intensity. A 3D point cloud with N points is formulated as $\mathbf{P} = \{\mathbf{p}_1, \mathbf{p}_2, \dots, \mathbf{p}_N\}$ where $\mathbf{p}_i \in \mathbb{R}^D$ for $i = 1, 2, \dots, N$, and D denotes attributes. In this work, we only consider 3D coordinates, in other words, $D = 3$. Point cloud data have two main distinct properties:

- Unorganized.

As a collection of 3D points coordinates, point clouds are different from structured images or volumetric grids, without the specific order. Thus, with any permutation

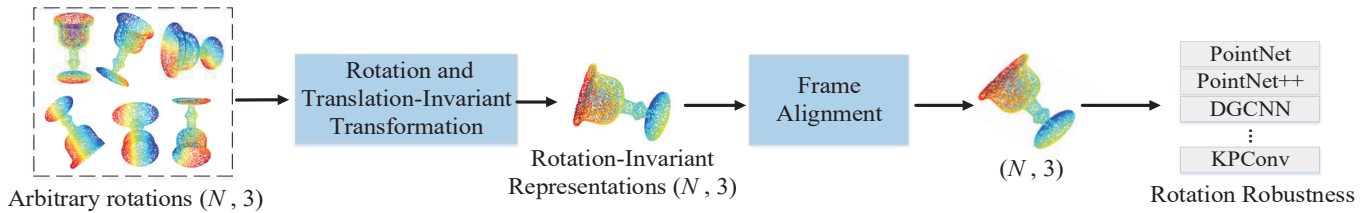


Fig. 1. Illustration of Self Contour-based Transformation architecture consisting of two novel modules: Rotation and Translation-Invariant Transformation and Frame Alignment. Point clouds are transformed by these two modules to obtain rotation-invariant representations and subsequently fed into existing techniques.

operations, point clouds still stand the same object, maintaining geometry topology.

- Rotation and Translation Invariance.

Point clouds are discrete representations of continuous surfaces of 3D space, indicating that under arbitrary rotations and translations, these rigid transformations should not change the semantic category of the object nor the intrinsic structures. Since the point cloud processing models need rotation and translation robustness.

For point cloud recognition tasks, the distribution of 3D point clouds needs to be modeled. Specifically, we adopt a deep network to learn the high-dimensional latent representations of point clouds that preserve the original point clouds' geometry structures and semantic features for further applications, e.g., classification and segmentation. Learning latent representations of point clouds module is also called a feature extraction network. Let Φ denotes a Feature Extraction Network, $\Phi : \mathbb{R}^{N \times 3} \rightarrow \mathbb{R}^C$

$$F = \Phi(P) \in \mathbb{R}^C, \quad (1)$$

where F is a C -dimensional vector descriptor, reflecting the original point clouds' semantic features. Then through a classifier f , we can get the output label.

$$l = f(F) \in \mathbb{R}^L, \quad (2)$$

where l denotes the predicted category label of original point cloud object.

Many recent proposed state-of-the-art techniques have achieved more than 92% accuracy on ModelNet40 [5], depending on effective feature extraction networks. Considering the perturbations of rotation and translation, the process of feature extraction are reformulated as:

$$F = \Phi(RP + T) \in \mathbb{R}^C, \quad (3)$$

where $R \in SO(3)$ represents a rotation matrix and T stands a translation matrix. However, the existing feature extraction models fail to learn rotation-invariant shape-awareness. Thus their performances degrade severely under random rotations, lacking rotation robustness, shown in Fig 2. To enhance the rotation and translation robustness and utilize the existing point cloud processing networks, we propose Self Contour-based Transformation architecture.

As illustrated in Fig 1, Self Contour-based Transformation (SCT) handles the arbitrary orientations points and maps them to rotation and translation-invariant representations which can be directly and flexibly processed by a variety of existing start-of-the-art point cloud recognition methods for classification

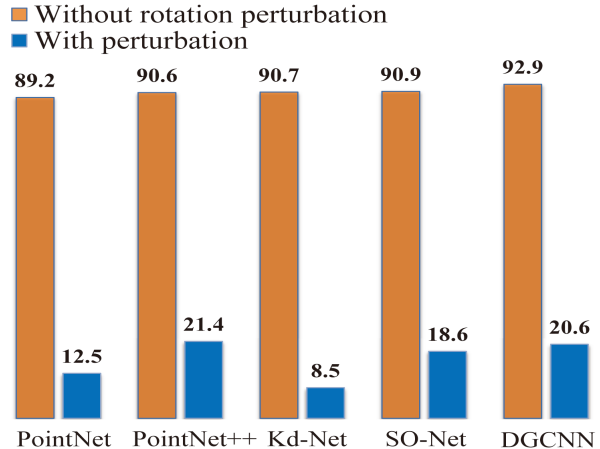


Fig. 2. Classification accuracy (%) on ModelNet40 with or without rotation perturbations. It is clear that the performances of existing point cloud processing models drop sharply under rotation. More comparison experiments are presented in Section V.

and segmentation tasks while keeping rotation and translation invariance.

SCT consists of two modules:

- 1) Rotation and Translation-Invariant Transformation. A Rotation and Translation-Invariant Transformation (RTIT) module transforms Cartesian coordinates of points to the rotation and translation-invariant representations.
- 2) Frame Alignment. A Frame Alignment (FA) module that enhances point clouds by detecting the contour points and regresses three axes alignment angles. The angles are extended to a coordinate system alignment matrix, aiming to transform each object from its self contour-based frame to an intra-class frame where discriminative features are easier to extract.

B. Rotation and Translation-Invariant Transformation (RTIT)

Given a point matrix $P = (\mathbf{p}_1, \mathbf{p}_2, \dots, \mathbf{p}_N)$ where $\mathbf{p}_i = (x_i, y_i, z_i)^T \in \mathbb{R}^3$ for $i = 1, 2, \dots, N$ in Cartesian frame, RTIT aims to transform the point clouds to the rotation and translation-invariant representations. To perform RTIT, a strictly RTIT is described to a one-to-one mapping G such that

$$G(RP + T) = G(P), \quad (4)$$

where $R \in SO(3)$ denotes a rotation matrix and $T = (\mathbf{t}, \mathbf{t}, \dots, \mathbf{t})$ is a $3 \times N$ translation matrix for $\mathbf{t} \in \mathbb{R}^3$. Since the point set P is sensitive to rotation and translation transformations, it is reasonable to find a proper

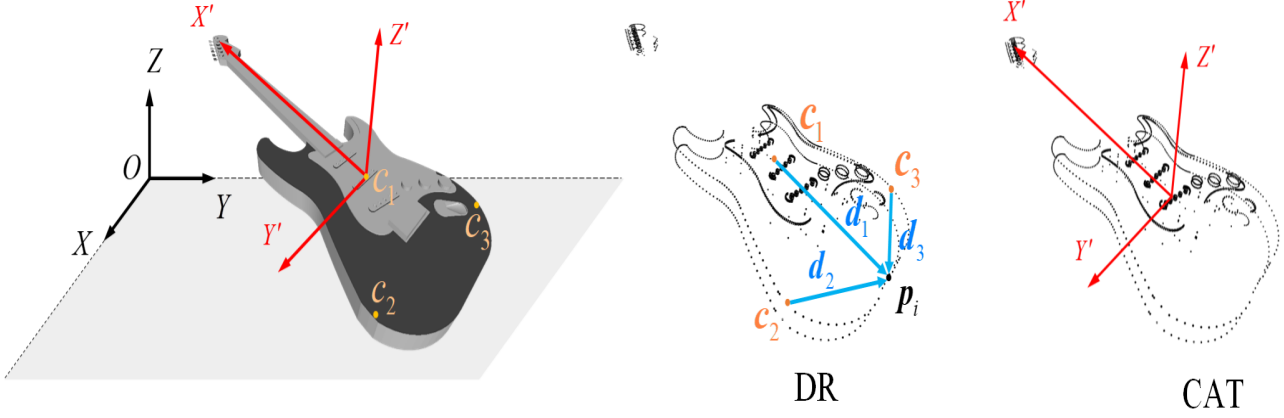


Fig. 3. Illustration of Rotation and Translation-Invariant Transformation (RTIT). RTIT includes two different approaches, Distances Relocalization (DR) and Contour-Aware Transformation (CAT).

RTIT to eliminate the effect of rotation transformation for a given point set P without information loss. To obtain a RTIT of point clouds, we propose two different approaches as follows:

a) *Distances Relocalization (DR)*: The combination of rotation and translation constitutes the rigid transformation, which preserves the relative distance of each point. Intuitively, the relative relationship of points is invariant to rotation and translation. Thus, we propose the DR method that converts each point coordinate to a relative distance-based representation. As the data preprocessing of PointNet [8], the point clouds are normalized into a unit sphere. Then three anchor points c_1, c_2 and c_3 are selected from point set P (orange points in Fig.3). For each point $p_i \in P$ (black point in Fig.3), distances between the three anchor points (blue lines in Fig.3) are computed and are viewed as new representations keeping rotation and translation invariance.

Specifically, the representation for a 3D point generated by DR is

$$\mathbf{p}'_i = (d_{i1}, d_{i2}, d_{i3})^T, \quad (5)$$

where $d_{ij} = \|\mathbf{p}_i - \mathbf{c}_j\|_2, j = 1, 2, 3$. It is obvious that the norm $\|\cdot\|_2$ is a rotation-invariant mapping for vectors with

$$\|R\mathbf{p}\|_2^2 = \|\mathbf{p}\|_2^2, \forall \mathbf{p} \in \mathbb{R}^3. \quad (6)$$

Based on the above formulation, the DR is a RTIT, which is formalized as the proposition below.

Proposition 1. *The DR transformation $G_{DR} : P \rightarrow P'$ satisfies the definition of RTIT such that $P' = G_{DR}(P) = G_{DR}(RP + T)$ holds for all translation $\mathbf{t} \in \mathbb{R}^3$ and rotation mapping $R \in SO(3)$.*

Proof. Let $\bar{P} = RP + T = (\bar{\mathbf{p}}_1, \bar{\mathbf{p}}_2, \dots, \bar{\mathbf{p}}_N)$ denotes point set transformed by the rotation matrix R and the translation matrix T . The element of new representation $\bar{\mathbf{p}}'_i$ transformed from $\bar{\mathbf{p}}_i$ is $\bar{d}_{ij} = \|\bar{\mathbf{p}}_i - \bar{\mathbf{c}}_j\|_2$ for $j = 1, 2, 3$ where $\bar{\mathbf{c}}_j = R\mathbf{c}_j + \mathbf{t}$.

Since $\|\cdot\|_2$ is rotation-invariant such that

$$\begin{aligned} \bar{d}_{ij} &= \|\bar{\mathbf{p}}_i - \bar{\mathbf{c}}_j\|_2 \\ &= \|R\mathbf{p}_i + \mathbf{t} - R\mathbf{c}_j - \mathbf{t}\|_2 \\ &= \|R(\mathbf{p}_i - \mathbf{c}_j)\|_2 \\ &= d_{ij}. \end{aligned} \quad (7)$$

Furthermore, let $P' = (\mathbf{p}'_1, \dots, \mathbf{p}'_N)$. Generally, for all points, we have $P' = G_{DR}(P) = G_{DR}(RP + T)$, which completes the proof and means P' has rotation and translation invariance concerning the given point set P through DR transformation. Moreover, the DR is a one-to-one correspondence mapping that can be mathematically proved.

To guarantee the rotation and translation invariance and preserve the structural information, the anchor points have to be fixed and uniquely recognized. The detailed procedure of selecting anchor points will be elaborated in Section IV.

b) *Contour-Aware Transformation (CAT)*: The DR converts the independent coordinates to relative distance-based representations through a nonlinear transformation to harvest rotation and translation invariance. Different from the linear transformation, the nonlinear transformation disturbs the data distribution inevitably. Inspired by the works on point set registration [51], [52] that linearly align two rigid transformed point sets, we aim to eliminate the effects of rotation and translation by a linear transformation. Then, the CAT is proposed to find three self contour-aware axes and transforms the frame to harvest rotation and translation-invariant representations. Before calculating the three orthogonal axes, the adjoint map [17] is given as below:

$$[(R\mathbf{x}) \times] = R[\mathbf{x} \times]R^T, \text{ for } R \in SO(3), \quad (8)$$

where $\mathbf{x} = (x_1, x_2, x_3)^T$ and $[\mathbf{x} \times]$ is the cross product matrix, defined by

$$[\mathbf{x} \times] = \begin{bmatrix} 0 & -x_3 & x_2 \\ x_3 & 0 & -x_1 \\ -x_2 & x_1 & 0 \end{bmatrix} \quad (9)$$

A proof of the above adjoint map is given in Appendix. The composite operation $(R\alpha_1) \times (R\alpha_2)$ is equal to $R(\alpha_1 \times \alpha_2)$, where $\alpha_1 = (x_1, y_1, z_1)^T$, $\alpha_2 = (x_2, y_2, z_2)^T$. According to Eq. (8), the proof is shown as below:

$$\begin{aligned} (R\alpha_1) \times (R\alpha_2) &= [(R\alpha_1) \times] R\alpha_2 \\ &= R[\alpha_1 \times] R^T R\alpha_2 \\ &= R(\alpha_1 \times \alpha_2) \end{aligned} \quad (10)$$

Eq. (10) provides the consistency under rotation. We calculate the barycenter of the points:

$$\mathbf{p}_b = \frac{1}{n} \sum_{i=1}^n (\mathbf{p}_i) = (x_b, y_b, z_b)^T, \quad (11)$$

the farthest point from barycenter:

$$\mathbf{p}_f = (x_f, y_f, z_f)^T = \arg \max_{\mathbf{p}_i \in P} \|\mathbf{p}_i - \mathbf{p}_b\|_2, \quad (12)$$

and the closest point from barycenter:

$$\mathbf{p}_c = (x_c, y_c, z_c)^T = \arg \min_{\mathbf{p}_i \in P} \|\mathbf{p}_i - \mathbf{p}_b\|_2. \quad (13)$$

Then, we define vector β_f , β_c and β_n , respectively.

$$\begin{aligned} \beta_f &= (x_f - x_b, y_f - y_b, z_f - z_b)^T, \\ \beta_c &= (x_c - x_b, y_c - y_b, z_c - z_b)^T, \\ \beta_n &= \beta_c \times \beta_f, \end{aligned} \quad (14)$$

where \times is cross product. To construct orthogonal axes, the vector β_c is finally updated, $\beta_c = \beta_f \times \beta_n$. Then these three vectors are scaled to unit norm:

$$\begin{aligned} \beta_f &= \beta_f / \|\beta_f\|, \\ \beta_n &= \beta_n / \|\beta_n\|, \\ \beta_c &= \beta_c / \|\beta_c\|. \end{aligned} \quad (15)$$

Then we generate a new self contour-aware frame B (As shown in Fig.3)

$$B = [\beta_f \ \beta_n \ \beta_c] = [X' \ Y' \ Z'], \quad (16)$$

and the point set P is accordingly transformed into

$$P' = G_{CAT}(P) = B^T(P - P_b), \quad (17)$$

where $P_b = (\mathbf{p}_b, \dots, \mathbf{p}_b)$ is a $3 \times N$ point matrix. The following proposition shows that we can use the CAT to generate rotation and translation-invariant representations.

Proposition 2. *The CAT mapping $G_{CAT} : P \rightarrow P'$ satisfies the definition of RTIT such that $P' = G_{CAT}(P) = G_{CAT}(RP + T)$ holds for all translation $\mathbf{t} \in \mathbb{R}^3$ and rotation mapping $R \in SO(3)$.*

Proof. Let $\bar{P} = RP + T = (\bar{\mathbf{p}}_1, \bar{\mathbf{p}}_2, \dots, \bar{\mathbf{p}}_N)$, then we have

$$\begin{aligned} \bar{B} &= (\bar{\beta}_f, \bar{\beta}_n, \bar{\beta}_c) \\ &= (\bar{\beta}_f, \bar{\beta}_c \times \bar{\beta}_f, \bar{\beta}_f \times (\bar{\beta}_c \times \bar{\beta}_f)), \end{aligned} \quad (18)$$

and,

$$\bar{\beta}_f = \bar{\mathbf{p}}_f - \bar{\mathbf{p}}_b = R(\mathbf{p}_f - \mathbf{p}_b) = R\beta_f, \quad (19)$$

$$\begin{aligned} \bar{\beta}_n &= \bar{\beta}_c \times \bar{\beta}_f \\ &= R(\beta_c - \beta_b) \times R(\beta_f - \beta_b) \\ &= R\beta_c \times R\beta_f. \end{aligned} \quad (20)$$

Considering Eq. (10) and Eq. (14), we have

$$R\beta_c \times R\beta_f = R(\beta_c \times \beta_f) = R\beta_n. \quad (21)$$

Eq. (20) reduces to

$$\bar{\beta}_n = R\beta_n. \quad (22)$$

Similarly, we have

$$\bar{\beta}_c = \bar{\beta}_f \times (\bar{\beta}_c \times \bar{\beta}_f) = R[\beta_f \times (\beta_c \times \beta_f)] = R\beta_c. \quad (23)$$

Substituting Eq. (19), Eq. (22), and Eq. (23) into Eq. (18), and yield

$$\bar{B} = (\bar{\beta}_f, \bar{\beta}_n, \bar{\beta}_c) = R(\beta_f, \beta_n, \beta_c) = RB. \quad (24)$$

Thus, the new representations with the novel G_{CAT} mapping are

$$\begin{aligned} \bar{P}' &= G_{CAT}(\bar{P}) \\ &= \bar{B}^T(\bar{P} - \bar{P}_b) \\ &= B^T R^T [RP - T - RP_b + T] \\ &= B^T(P - P_b). \end{aligned} \quad (25) \quad \square$$

The technical results shown in Proposition 2 indicates that $P' = G_{CAT}(P) = G_{CAT}(RP + T)$, which means P' also keeps strict rotation and translation invariance concerning the given point set P through linear CAT mapping.

The detailed experiments in Section V will demonstrate that the versatile RTIT is efficient and effective for synthetic and real benchmarks.

C. Frame Alignment (FA)

The previous RTIT module transforms points from the Cartesian Coordinate to each self contour-based frame to obtain rotation and translation invariance. However, the feature extraction network has to learn discriminative features across different frames instead of the unified Cartesian Coordinate, which is much more difficult. To address the problem, for each rotation and translation-invariant representation provided by RTIT, we leverage a Frame Alignment (FA) module to capture contours and transform its self contour-based frame to an intra-class frame to enhance discriminative feature extraction. As shown in Fig. 4, FA consists of two modules: Contour Encoding and Frame Transformation Regression.

a) *Contour Encoding:* Given the rotation and translation-invariant representations P' , this unit explicitly captures the contours and augments these points through a self-attention mechanism, which explores the geometric structure and eventually benefits the entire model. To this end, the operation is formulated as:

$$f_c = \sigma(\phi(P')), P' \in \mathbb{R}^{N \times 3}, \quad (26)$$

$$P'_c = softmax(\phi(f_c)), P'_c \in \mathbb{R}^{N \times 3}, \quad (27)$$

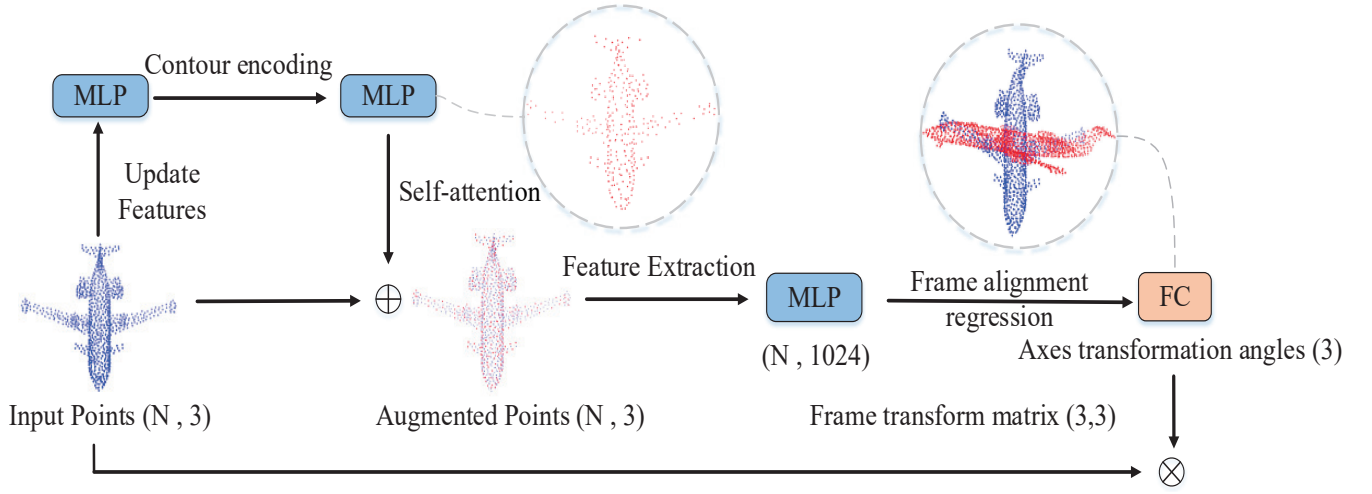


Fig. 4. Architecture of Frame Alignment (FA). FA consists of Contour Encoding and Frame Transformation Regression.

where σ is a nonlinear activator and ϕ is chosen as a multi-layer perceptron (MLP). The first MLP maps points from three-dimension space to a high-dimensional space and harvests latent representations. Then we employ another MLP to reduce feature dimensions to 3D, preserving salient features. Finally, a softmax function is used to figure out key points. We enhance the rotation and translation-invariant representations P' with contour features P'_c , resulting in augmented representations P'_a ,

$$P'_a = P' \oplus P'_c, \quad (28)$$

where \oplus denotes channel-wise summation.

b) *Frame Transformation Regression*: The Frame Transformation Regression transforms point clouds from its self contour-based frame to an intra-class frame. A straightforward way to generate a transformation matrix is to use point clouds, augmented by the Contour Encoding module, as the input of Frame Transformation Regression. The overview of our Frame Transformation Regression is in Fig. 4. The proposed architecture follows the encoder-decoder framework. For the encoder, we adopt a simply PointNet-like [8] 1024-dimensional vector descriptor with a maximum pooling function, resulting in global features f_{global} . Afterward, several fully connected layers are used as a decoder to regress three frame transformation angles, which are further extended to a 3x3 transformation matrix. Mathematically, the pipeline of FA is formulated as

$$f_{global} = \mathcal{A}(\gamma(P'_a)) \in \mathbb{R}^C, \quad (29)$$

$$[\beta_1, \beta_2, \beta_3] = \theta(f_{global}) \in \mathbb{R}^3, \quad (30)$$

where P'_a is the points augmented by Contour Encoding, γ denotes PointNet-like [8] 1024-dimensional vector descriptor, \mathcal{A} stands aggregation function, max-pooling, and θ is the fully connected layers to regress three transformation angles. Finally, the transformation matrix T_{est} can be described as

$$T_{est} = T_3 \cdot T_2 \cdot T_1, \quad (31)$$

where

$$T_1 = \begin{bmatrix} 1 & 0 & 0 \\ 0 & \cos\beta_1 & \sin\beta_1 \\ 0 & -\sin\beta_1 & \cos\beta_1 \end{bmatrix},$$

$$T_2 = \begin{bmatrix} \cos\beta_2 & 0 & -\sin\beta_2 \\ 0 & 1 & 0 \\ \sin\beta_2 & 0 & \cos\beta_2 \end{bmatrix},$$

$$T_3 = \begin{bmatrix} \cos\beta_3 & \sin\beta_3 & 0 \\ -\sin\beta_3 & \cos\beta_3 & 0 \\ 0 & 0 & 1 \end{bmatrix}.$$

However, it is a complex problem, and the regression result is easily trapped into the local optimum. To overcome this issue, we modify the loss function, adding an alignment loss $L_{alignment}$ which aims to minimize the difference between the estimated frame transformation T_{est} and the ground truth frame transformation T_{gt} .

$$L_{alignment} = \|T_{est} - T_{gt}\|_2. \quad (32)$$

$T_{gt} = B^T$ and B is calculated by Eq. (16) which is a rotation matrix. Finally, the total loss is formulated:

$$L = L_{cls} + \lambda L_{alignment}, \quad (33)$$

where λ denotes weight to balance each term. A small λ encourages the model to focus more on the classification with less attention on frame alignment, and vice versa. In this paper, we set $\lambda = 0.01$.

IV. DISCUSSIONS AND COMPLEXITY ANALYSIS

In this section, we give a discussion and complexity analysis of our self contour-based approach.

A. Rotation and Translation-Invariant Transformation

Rotation-invariant transformation methods are the critical component in existing rotation-invariant architectures. Therefore, we compare and analyze their performances and time complexity in this section.

TABLE I
PERFORMANCE COMPARISONS OF ROTATION INVARIANT
TRANSFORMATION METHODS ON MODELNET40. * DENOTES OUR
METHODS.

| Method | Accuracy | Type |
|------------------------|-------------|------|
| DR* + DGCNN | 85.1 | NT |
| SRINet [21]+ DGCNN | 86.1 | NT |
| ClusterNet [20]+ DGCNN | 86.4 | NT |
| CAT* + DGCNN | 88.8 | LT |

TABLE II
COMPARISON OF TIME COMPLEXITY. * DENOTES OUR METHODS. NT
AND LT REPRESENTS NONLINEAR AND LINEAR TRANSFORMATION,
RESPECTIVELY.

| Method | Time complexity | Type |
|-----------------|-----------------|------|
| DR* | $O(N)$ | NT |
| SRINet [21] | $O(N)$ | NT |
| ClusterNet [20] | $O(NK)$ | NT |
| CAT* | $O(N)$ | LT |

- SRINet [18] chooses three axes and maps each point into a collection of relative angles and leverages a key point detection module to improve performance.
- ClusterNet [20] builds K-nearest neighbor graphs and transform Cartesian coordinates into relative angles and norms to obtain rotation invariance. Then, it utilizes a clustering operation to extract features, which is time-consuming and not applicable to the segmentation task.

Nonlinear rotation-invariant transformation methods include ClusterNet [20], SRINet [18] and our Distances Relocalization (DR). Specifically, we select four fixed anchors points in the DR method. Thus, we calculate the barycenter of a point set, the farthest, the second farthest point, and the closest point of the barycenter, as the four unique recognized anchors. In contrast, Contour-Aware Transformation (CAT) is a linear function visualized in Fig 5. To show the effectiveness of proposed RTIT, we test and compare these rotation-invariant transformation methods under ModelNet40 [5]. For a fair comparison, we choose DGCNN [10] as the backbone of these transformation approaches. The qualitative and quantitative evaluation results are summarized in Table I and Table II. NT and LT represent nonlinear and linear transformation, respectively.

The linear transformation method CAT outperforms other methods. Though ClusterNet builds local graphs and encodes relative angles, it is still suffering from the loss of geometry information. Due to global linear transformation, CAT leads the performance under arbitrary rotation conditions with lower time complexity.

B. Discussion about Frame Alignment Module

The aim here is to demonstrate that Frame Alignment is a key part of our architecture. Under arbitrary rotations and

translations, these rigid transformations should not change the semantic category of the 3D object nor intrinsic geometry structures. The RTIT module generates a rotation and translation-invariant representations at the cost of transforming The Cartesian frame to self contour-based frame. To alleviate the issue, we need a coordinate system alignment matrix, aiming to transform each object from its self contour-based frame to an intra-class frame. T-net proposed in PointNet [8] predicts a affine transformation matrix for feature alignment. However, nonlinearly affine transformation harms geometry relation and suffers from information loss inevitably, which is not applicable to this work. For coordinate frame alignment purpose, the transformation matrix should be a rotation matrix. Thus, the FA module is introduced.

The point clouds transformed by FA is visualized in Fig. 6. The input and output of FA are blue and red, respectively. We see that the frame alignment transformations of various objects are different. For the same category, FA transforms two lamps differently. This indicates that the FA generates a contour-based transformation matrix to ease feature extraction. Furthermore, the ablation study in Table VI shows that FA gives another 0.5% boost in classification accuracy, which demonstrates its effectiveness again.

V. EXPERIMENTS

In this section, we conduct extensive experiments on several point cloud classification and part segmentation benchmark datasets including ModelNet40 [5], ScanObjectNN [53] and ShapeNet [54]. Some experimental results are visualized to demonstrate the effectiveness of the proposed technique. The point clouds transformed by SCT can be easily processed by the existing point cloud recognition architectures while maintaining rotation invariance, which is complementary to rotation robustness of various existing models. We further feed these transformed point clouds into the DGCNN [10] model for classification and part segmentation tasks under arbitrary rotations, and conduct ablation study. All the experiments are implemented on two NVIDIA TITAN Xp GPUs in a distributed manner. NR/NR represents training and testing without rotations. NR/AR denotes training without rotations augmentation while testing with arbitrary rotations.

A. Synthetic ModelNet40

We conduct the classification tasks on the ModelNet40 [5] dataset under arbitrary rotations which consists of 40 different categories with 9843 synthetic CAD training models and 2468 testing models. We uniformly sample 1024 points from models' surfaces to train our model. Following the experimental settings of PointNet [8], these sampled point clouds are translated and rescaled into a unit sphere later. As 3D sensors could not capture normals directly in the real world, only the (x,y,z) coordinates of the sampled points are used as the input of models. During the training process, random scaling and jittering are added to perturb points' original positions. Since our backbone employs DGCNN, the training strategy is almost the same as [10] expect that training epochs are changed to 290.

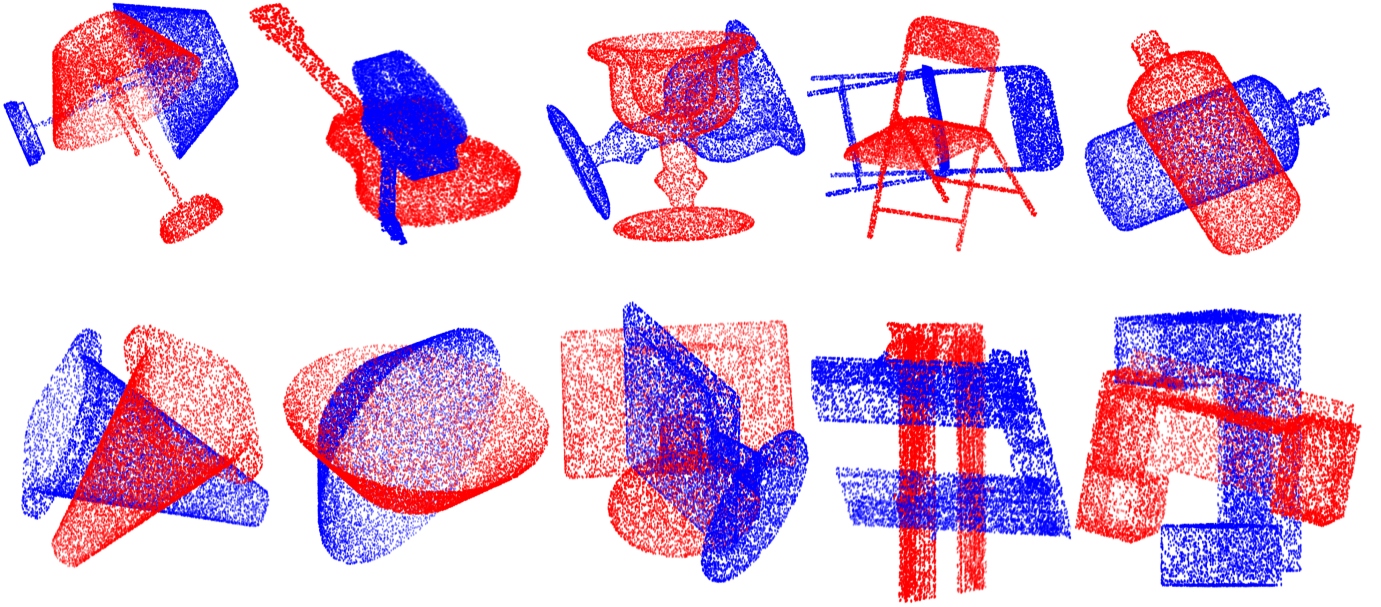


Fig. 5. Visualization of Contour-Aware Transformation (CAT). The original 3D objects and transformed by CAT are blue and red, respectively.

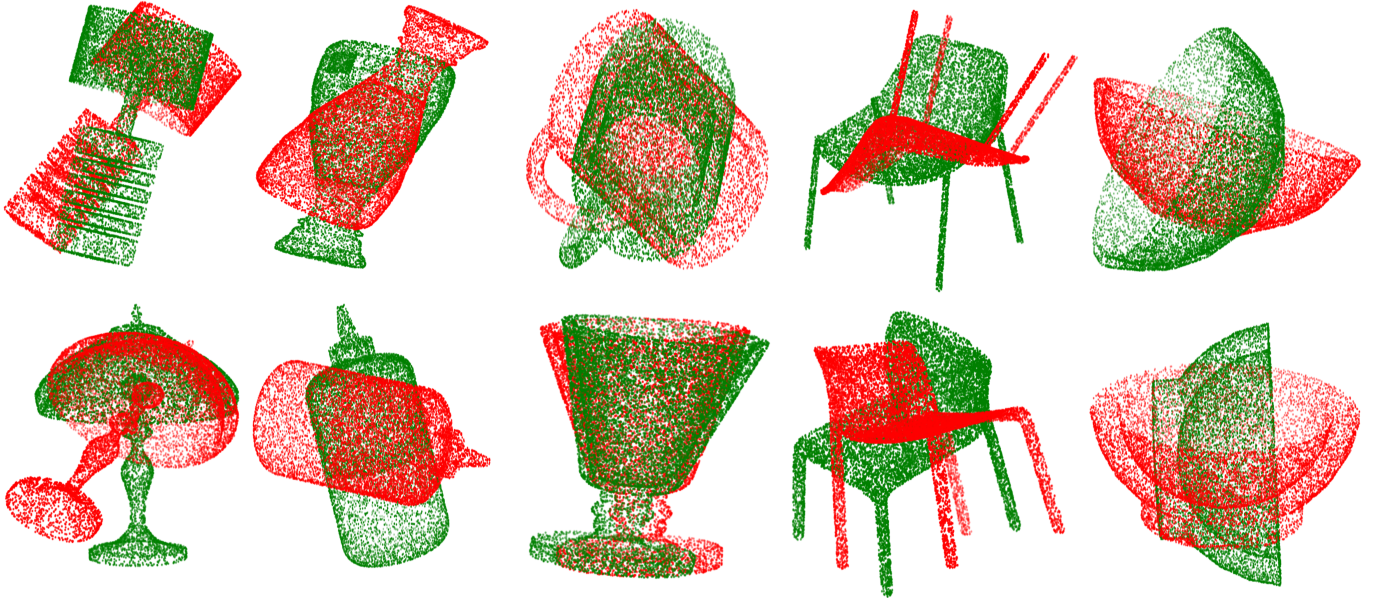


Fig. 6. Visualization of Frame Alignment (FA). The rotation and translation-invariant representations generated by CAT and 3D objects transformed by Frame Alignment are red and green, respectively.

Evaluation Table III shows the results without voting trick. Clearly, our method achieves the best accuracy under random rotations on the ModelNet40 dataset. Though the recent point cloud recognition methods have harvested very high accuracy, their performances degrade severely with rotations perturbation, implying the vulnerability to the rotations. PointNet and DGCNN drop more than 70% classification accuracy under rotations, failing to generalize to arbitrary orientations. Compared with other rotation-invariant methods, our model is 2.3% better than ClusterNet [20] and SRINet [18].

Besides, the proposed method has a stable classification performance with/without the rotation augmentation, which also proves its rotation invariance.

B. Real-world ScanObjectNN

Different from synthetic benchmark ModelNet40 [5] dataset, ScanObjectNN [53] is a newly published real-world dataset comprising of 2902 3D objects in 15 categories. We implement the classification task on the ScanObjectNN [53] to further prove the robustness and generalization ability of our technique in real-world scenarios. The training strategy,

TABLE III
CLASSIFICATION RESULTS ON MODELNET40.

| Method | NR/NR | NR/AR | Δ Acc |
|-----------------|-------------|-------------|--------------|
| PointNet [8] | 89.2 | 12.5 | -76.7 |
| Kd-Net [14] | 90.7 | 8.5 | -82.2 |
| PointNet++ [9] | 90.6 | 21.4 | -69.2 |
| SO-Net [36] | 90.9 | 18.6 | -72.3 |
| DGCNN [10] | 92.9 | 20.6 | -72.3 |
| PRIN [18] | 80.1 | 70.4 | -9.7 |
| ClusterNet [20] | 87.1 | 87.1 | 0 |
| SRINet [21] | 87.1 | 87.1 | 0 |
| Our | 89.3 | 89.3 | 0 |

TABLE IV
CLASSIFICATION RESULTS ON SCANOBJECTNN.

| Method | NR/NR | NR/AR | Δ Acc |
|-----------------|-------------|-------------|--------------|
| PointNet [8] | 79.8 | 24.9 | -76.7 |
| Kd-Net [14] | 80.1 | 19.5 | -60.6 |
| PointNet++ [9] | 85.5 | 26.9 | -58.6 |
| DGCNN [10] | 86.2 | 27.2 | -59.0 |
| PointCNN [10] | 86.3 | 29.6 | -56.7 |
| PRIN [18] | 73.4 | 68.7 | -4.7 |
| ClusterNet [20] | 80.4 | 80.4 | 0 |
| Our | 82.5 | 82.5 | 0 |

network architecture and input settings are the same as the synthetic benchmark. For a fair comparison, all the experiments are conducted in "object only" of data split 1. NR/AR represents training without rotations augmentation while testing with arbitrary rotations. NR/NR stands training and testing without rotations.

Evaluation Note that SRINet [18] needs normal vectors as input, while ScanObjectNN do not contain normal attributes. Thus, we do not compare with SRINet in Table IV. Compared with the synthetic dataset, the real-world benchmark is more challenging, with a noticeable performance drop. Nevertheless, our method outperforms the others by a large margin under random rotations. As shown in IV, the proposed model surpasses other rotation-invariant techniques and improves rotation robustness of the existing models, advancing ClusterNet [20] by 2.1%. The consistent performances on synthetic and real-world datasets show the generalization and robustness of our model. Demonstrating its potential applications in the practical point cloud registration task with arbitrary rotations.

C. ShapeNet

In this section, we conduct our method for part segmentation task on ShapeNet part [54] dataset containing 16,881 3D objects from 16 categories and 50 annotated parts in total. Part segmentation is a fine-grained classification task, aiming to assign a semantic label to each point of a 3D object. Each object contains less than 6 part category labels. We randomly sample 2048 points from each object and split the dataset into train, validation and test part as the official scheme. The training strategy adopted for part segmentation is the same as the classification task. To compare with state-of-the-art point cloud recognition architectures under arbitrary rotations, we train and test models with three different settings. 1. Models are trained and tested without rotation (NR/NR). 2. Models are trained without rotation augmentation and tested with arbitrary rotations (NR/AR). 3. Arbitrary rotations are added during both training and testing process (AR/AR).

Evaluation For a fair comparison, we use the mean Intersection-over-Union (mIoU) metric proposed in PointNet. The results of our method and other techniques are shown in Table V without the voting trick. Note that ClusterNet [20] is dedicated to classification and not applicable to part segmentation application. Those state-of-the-art models lack the rotation robustness, failing to classify each part of the object with sharp performances drop under rotations (Fig 8). In our experiments, training with rotation augmentation gives PointNet++ and DGCNN an approximately 20% boost in mIoU, achieving 58% and 62.7%, respectively. Though rotation augmentation slightly improves their rotation robustness, there is still a performance gap between those models and our method. Moreover, the comparison of classification results shown in Table V demonstrates that the proposed method outperforms other rotation-invariant methods, achieving 82.5% mIoU.

D. Ablation Study

In this section, we conduct an ablation study of Self Contour-based Transformation to figure out how each module affects the overall performance. All the experiments are implemented on ModelNet40 [5] against rotations, and the performance metric is the accuracy (%). Models are trained without rotation augmentation and tested under arbitrary rotations. Table VI illustrates the results of the ablation study with (x, y, z) coordinates. The baseline (Model A) denotes DGCNN [10], only remaining a classification accuracy of 20.6%. When employed with our DR, it obtains rotation invariance and is improved to 85.1% (model B). Besides, we also apply the CAT with DGCNN (model C) which outperforms DR methods, avoiding impairing global structure. Moreover, the use of FA (model D) gives model C another 0.5% boost and achieves state-of-the-art under arbitrary rotations.

Comparing the performances of models A, B, C, and D, it is evident that both DR, CAT and FA improve rotation robustness. We train the model with 2,048 points (Model E) to figure out the impact of input size on performance but find no boost. It is convinced that, compared with increasing

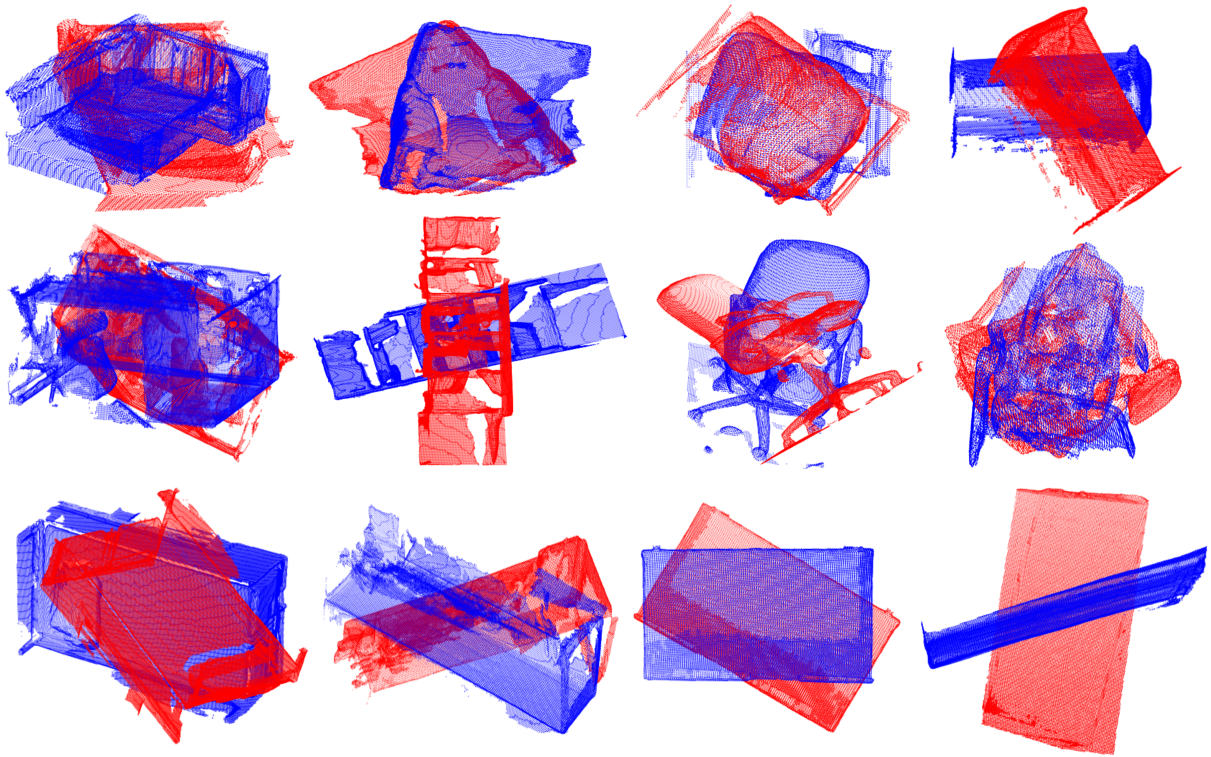


Fig. 7. Rotation and translation-invariant representations generated by Contour-Aware Transformation on ScanObjectNN. With the presence of occlusions and background, real-world scanned objects contains more irregular shapes.

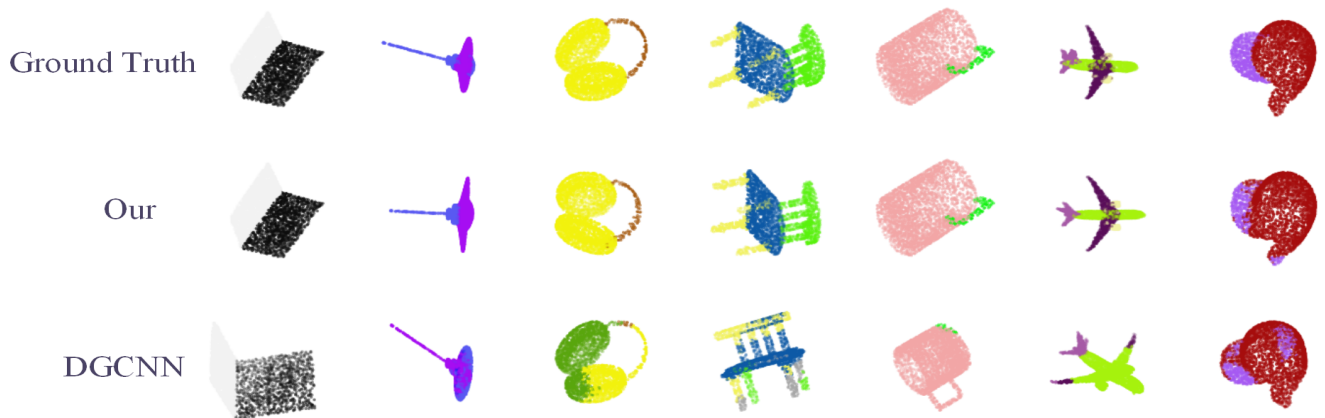


Fig. 8. Visualization of part segmentation results on ShapeNet under arbitrary rotations.

TABLE V
PART SEGMENTATION RESULTS ON SHAPENET DATASET. METRIC IS MEAN IOU(%).

| Method | Input | NR/NR | NR/AR | Δ mIoU | AR/AR | Δ mIoU |
|----------------|-----------------|-------------|-------------|---------------|-------------|---------------|
| PointNet [8] | 2048×3 | 83.2 | 31.3 | -51.9 | 50.7 | -32.5 |
| PointNet++ [9] | 2048×3 | 84.6 | 36.7 | -47.9 | 58.0 | -26.6 |
| SO-Net [36] | 2048×3 | 84.8 | 27.3 | -57.5 | 57.8 | -27.0 |
| DGCNN [10] | 2048×3 | 84.7 | 43.8 | -40.9 | 62.7 | -22.0 |
| PRIN [18] | 2048×3 | 71.5 | 57.4 | -14.1 | 68.9 | -2.6 |
| SRINet [21] | 2048×3 | 77.0 | 77.0 | 0 | 77.0 | 0 |
| Our | 2048×3 | 81.4 | 81.4 | 0 | 81.4 | 0 |

TABLE VI
ABLATION STUDY. ALL THE EXPERIMENTS ARE IMPLEMENTED ON MODELNET40 [5] AGAINST ROTATIONS. INCREASING POINTS NUMBER DOES NOT BOOST CLASSIFICATION ACCURACY.

| Method | #points | DR | CAT | FA | Acc(%) |
|--------|---------|----|-----|----|--------|
| A | 1k | | | | 20.6 |
| B | 1k | ✓ | | | 85.1 |
| C | 1k | | ✓ | | 88.8 |
| D | 1k | | ✓ | ✓ | 89.3 |
| E | 2k | | ✓ | ✓ | 89.3 |

TABLE VII
HYPER-PARAMETER ANALYSIS. EXPERIMENTS ARE CONDUCTED ON MODELNET40 UNDER ROTATION PERTURBATIONS.

| λ | #points | Acc(%) |
|-----------|---------|--------|
| 0.001 | 1k | 89.0 |
| 0.008 | 1k | 89.1 |
| 0.01 | 1k | 89.3 |
| 0.02 | 1k | 89.1 |

input size, using an efficient and information-lossless rotation-invariant transformation is more cost-effective to extract the discriminative features against arbitrary rotations.

E. Hyper-parameter Analysis

The different classification accuracies with choices of λ in Eq. (33) is shown in Table VII. As aforementioned in Section III-C, a small λ encourages the model to focus more on the classification with less attention on frame alignment. However, if λ is too small, e.g., 0.001, the frame alignment module tends to keep static, thus leading to a local optimal minimum, resulting in a worse performance; On the other hand, a too-large λ , e.g., 0.02, the feature extraction process tends to be omitted, hindering the classification network training. In this work, we set $\lambda = 0.01$ to balance each term.

F. Robustness Evaluation

The robustness of our RTIT on sampling density is shown in Fig 10. We test the CAT with sparser points of 1024, 768, 512, and 256 and visualize those results in Fig 9. For a fair comparison, all the RTIT methods are fed into the DGCNN model. Note that we do not use random input dropout augmentation during training. Visualization results in Fig 9 demonstrates that CAT consistently transforms points based on contours under different sampling densities. Fig 10 shows that our CAT is more robust than other methods. The interpretation is that nonlinear transformation techniques rely on local geometry structures, which are more sensitive to density differences while linear CAT focuses on global shape harvesting robustness.

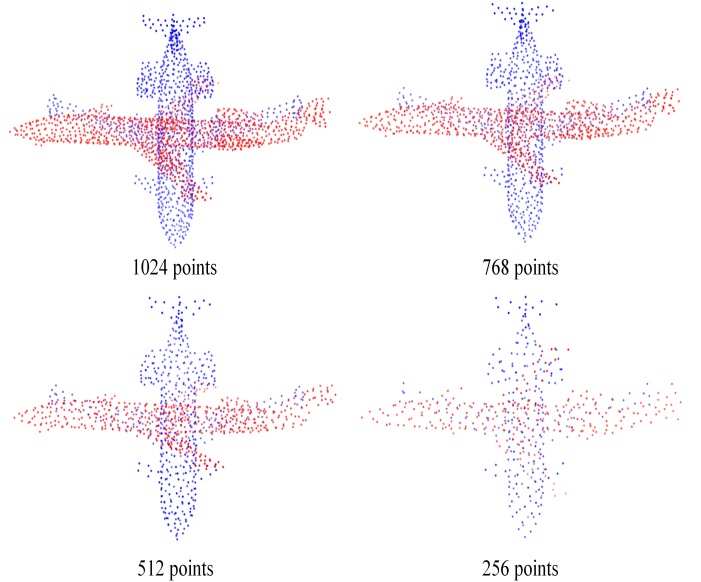


Fig. 9. Rotation-Invariant Transformation methods under different sampling densities. Blue stands original points and red denotes transformed points by CAT approach.

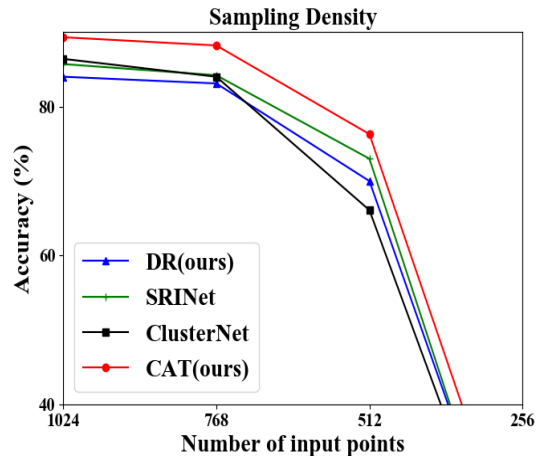


Fig. 10. Classification accuracy under different sampling densities.

VI. CONCLUSION

In this paper, a novel SCT module has been proposed for point cloud recognition against arbitrary rotations, which can be flexibly integrated into various point cloud processing networks. SCT provides efficient and strictly rotation and translation invariance by introducing RTIT. It transforms Cartesian coordinates of points to the self contour-based rotation and translation-invariant representations while maintaining the global geometric structure. Moreover, a FA module has been proposed to capture contours and transform self contour-based frames to the intra-class frame to enhance discriminative shape awareness extraction. Various experiments have been conducted to verify the effectiveness and efficiency of the SCT and the experimental results demonstrate that, with the above two modules, SCT achieves state-of-the-art performance on the tasks of classification and part segmentation on synthetic and real-world datasets against arbitrary rotations. Besides, SCT

with its rotation invariance and efficiency can be applied in real-world point cloud processing applications which are always accompanied by random rotations.

APPENDIX

For $\mathbf{x} = (x_1, x_2, x_3)^T$ and $\mathbf{y} = (y_1, y_2, y_3)^T$, the inner product is given by,

$$\mathbf{x} \cdot \mathbf{y} = \mathbf{x}^T \mathbf{y} = \mathbf{y}^T \mathbf{x}. \quad (\text{A.1})$$

It is convenient to express matrix in terms of its columns. For a 3x3 matrix $M \equiv [\mathbf{a} \ \mathbf{b} \ \mathbf{c}]$, the adjoint [17] is

$$\text{adj}M = \text{adj}([\mathbf{a} \ \mathbf{b} \ \mathbf{c}]) = \begin{bmatrix} (\mathbf{b} \times \mathbf{c})^T \\ (\mathbf{c} \times \mathbf{a})^T \\ (\mathbf{a} \times \mathbf{b})^T \end{bmatrix} \quad (\text{A.2})$$

And $[\mathbf{x} \times]$ is the cross product matrix, defined by

$$[\mathbf{x} \times] = \begin{bmatrix} 0 & -x_3 & x_2 \\ x_3 & 0 & -x_1 \\ -x_2 & x_1 & 0 \end{bmatrix} \quad (\text{A.3})$$

Then

$$M^T [\mathbf{x} \times] M = \begin{bmatrix} \mathbf{a}^T (\mathbf{x} \times \mathbf{a}) & \mathbf{a}^T (\mathbf{x} \times \mathbf{b}) & \mathbf{a}^T (\mathbf{x} \times \mathbf{c}) \\ \mathbf{b}^T (\mathbf{x} \times \mathbf{a}) & \mathbf{b}^T (\mathbf{x} \times \mathbf{b}) & \mathbf{b}^T (\mathbf{x} \times \mathbf{c}) \\ \mathbf{c}^T (\mathbf{x} \times \mathbf{a}) & \mathbf{c}^T (\mathbf{x} \times \mathbf{b}) & \mathbf{c}^T (\mathbf{x} \times \mathbf{c}) \end{bmatrix} \quad (\text{A.4})$$

According to Eq. (A.1), Eq. (A.4) is equal to

$$\begin{aligned} M^T [\mathbf{x} \times] M &= \begin{bmatrix} \mathbf{a} \cdot (\mathbf{x} \times \mathbf{a}) & \mathbf{a} \cdot (\mathbf{x} \times \mathbf{b}) & \mathbf{a} \cdot (\mathbf{x} \times \mathbf{c}) \\ \mathbf{b} \cdot (\mathbf{x} \times \mathbf{a}) & \mathbf{b} \cdot (\mathbf{x} \times \mathbf{b}) & \mathbf{b} \cdot (\mathbf{x} \times \mathbf{c}) \\ \mathbf{c} \cdot (\mathbf{x} \times \mathbf{a}) & \mathbf{c} \cdot (\mathbf{x} \times \mathbf{b}) & \mathbf{c} \cdot (\mathbf{x} \times \mathbf{c}) \end{bmatrix} \\ &= \begin{bmatrix} 0 & -(\mathbf{a} \times \mathbf{b}) \cdot \mathbf{x} & (\mathbf{c} \times \mathbf{a}) \cdot \mathbf{x} \\ (\mathbf{a} \times \mathbf{b}) \cdot \mathbf{x} & 0 & -(\mathbf{b} \times \mathbf{c}) \cdot \mathbf{x} \\ -(\mathbf{c} \times \mathbf{a}) \cdot \mathbf{x} & (\mathbf{b} \times \mathbf{c}) \cdot \mathbf{x} & 0 \end{bmatrix} \end{aligned} \quad (\text{A.5})$$

Considering Eq. (A.2), and Eq. (A.3), Eq. (A.5) reduces to

$$M^T [\mathbf{x} \times] M = \{[(\text{adj}M)\mathbf{x}] \times\}. \quad (\text{A.6})$$

Setting $M = R^T$, when R is a proper orthogonal 3x3 matrix and adjacency matrix $\text{adj}M = R$ then

$$R[\mathbf{x} \times]R^T = [(R\mathbf{x}) \times], \text{ for } R \in SO(3). \quad (\text{A.7})$$

REFERENCES

- [1] R. B. Rusu and S. Cousins, "3d is here: Point cloud library (pcl)," in *2011 IEEE International Conference on Robotics and Automation*. IEEE, 2011, pp. 1–4.
- [2] J. Han, L. Shao, D. Xu, and J. Shotton, "Enhanced computer vision with microsoft kinect sensor: A review," *IEEE Transactions on Cybernetics*, vol. 43, no. 5, pp. 1318–1334, 2013.
- [3] Y. Guo, H. Wang, Q. Hu, H. Liu, L. Liu, and M. Bennamoun, "Deep learning for 3d point clouds: A survey," *IEEE Transactions on Pattern Analysis and Machine Intelligence*, 2020.
- [4] D. Maturana and S. Scherer, "Voxnet: A 3d convolutional neural network for real-time object recognition," in *2015 IEEE/RSJ International Conference on Intelligent Robots and Systems (IROS)*. IEEE, 2015, pp. 922–928.
- [5] Z. Wu, S. Song, A. Khosla, F. Yu, L. Zhang, X. Tang, and J. Xiao, "3d shapenets: A deep representation for volumetric shapes," in *Proceedings of the IEEE conference on computer vision and pattern recognition*, 2015, pp. 1912–1920.
- [6] Y. Feng, Y. Feng, H. You, X. Zhao, and Y. Gao, "Meshnet: Mesh neural network for 3d shape representation," in *Proceedings of the AAAI Conference on Artificial Intelligence*, vol. 33, 2019, pp. 8279–8286.
- [7] X. Chen, H. Ma, J. Wan, B. Li, and T. Xia, "Multi-view 3d object detection network for autonomous driving," in *Proceedings of the IEEE Conference on Computer Vision and Pattern Recognition*, 2017, pp. 1907–1915.
- [8] C. R. Qi, H. Su, K. Mo, and L. J. Guibas, "Pointnet: Deep learning on point sets for 3d classification and segmentation," in *Proceedings of the IEEE Conference on Computer Vision and Pattern Recognition*, 2017, pp. 652–660.
- [9] C. R. Qi, L. Yi, H. Su, and L. J. Guibas, "Pointnet++: Deep hierarchical feature learning on point sets in a metric space," in *Advances in neural information processing systems*, 2017, pp. 5099–5108.
- [10] Y. Wang, Y. Sun, Z. Liu, S. E. Sarma, M. M. Bronstein, and J. M. Solomon, "Dynamic graph cnn for learning on point clouds," *ACM Transactions on Graphics (TOG)*, vol. 38, no. 5, p. 146, 2019.
- [11] Q. Hu, B. Yang, L. Xie, S. Rosa, Y. Guo, Z. Wang, N. Trigoni, and A. Markham, "Randla-net: Efficient semantic segmentation of large-scale point clouds," in *Proceedings of the IEEE/CVF Conference on Computer Vision and Pattern Recognition*, 2020, pp. 11 108–11 117.
- [12] C. R. Qi, W. Liu, C. Wu, H. Su, and L. J. Guibas, "Frustum pointnets for 3d object detection from rgb-d data," in *Proceedings of the IEEE Conference on Computer Vision and Pattern Recognition*, 2018, pp. 918–927.
- [13] C. R. Qi, O. Litany, K. He, and L. J. Guibas, "Deep hough voting for 3d object detection in point clouds," in *Proceedings of the IEEE International Conference on Computer Vision*, 2019, pp. 9277–9286.
- [14] R. Klokov and V. Lempitsky, "Escape from cells: Deep kd-networks for the recognition of 3d point cloud models," in *Proceedings of the IEEE International Conference on Computer Vision*, 2017, pp. 863–872.
- [15] H. Thomas, C. R. Qi, J.-E. Deschaud, B. Marcotegui, F. Goulette, and L. J. Guibas, "Kpconv: Flexible and deformable convolution for point clouds," in *Proceedings of the IEEE International Conference on Computer Vision*, 2019, pp. 6411–6420.
- [16] J. Mao, X. Wang, and H. Li, "Interpolated convolutional networks for 3d point cloud understanding," in *Proceedings of the IEEE International Conference on Computer Vision*, 2019, pp. 1578–1587.
- [17] F. L. Markley and J. L. Crassidis, *Fundamentals of spacecraft attitude determination and control*. Springer, 2014, vol. 33.
- [18] Y. You, Y. Lou, Q. Liu, Y.-W. Tai, L. Ma, C. Lu, and W. Wang, "Pointwise rotation-invariant network with adaptive sampling and 3d spherical voxel convolution," in *AAAI*, 2020, pp. 12 717–12 724.
- [19] H. Deng, T. Birdal, and S. Ilic, "Ppf-foldnet: Unsupervised learning of rotation invariant 3d local descriptors," in *Proceedings of the European Conference on Computer Vision (ECCV)*, 2018, pp. 602–618.
- [20] C. Chen, G. Li, R. Xu, T. Chen, M. Wang, and L. Lin, "Clusternet: Deep hierarchical cluster network with rigorously rotation-invariant representation for point cloud analysis," in *Proceedings of the IEEE Conference on Computer Vision and Pattern Recognition*, 2019, pp. 4994–5002.
- [21] X. Sun, Z. Lian, and J. Xiao, "Srinet: Learning strictly rotation-invariant representations for point cloud classification and segmentation," in *Proceedings of the 27th ACM International Conference on Multimedia*, 2019, pp. 980–988.
- [22] Y. Rao, J. Lu, and J. Zhou, "Spherical fractal convolutional neural networks for point cloud recognition," in *Proceedings of the IEEE Conference on Computer Vision and Pattern Recognition*, 2019, pp. 452–460.
- [23] G. Riegler, A. Osman Ulusoy, and A. Geiger, "Octnet: Learning deep 3d representations at high resolutions," in *Proceedings of the IEEE Conference on Computer Vision and Pattern Recognition*, 2017, pp. 3577–3586.
- [24] R. Girshick, "Fast r-cnn," in *Proceedings of the IEEE international conference on computer vision*, 2015, pp. 1440–1448.
- [25] C. Choy, J. Gwak, and S. Savarese, "4d spatio-temporal convnets: Minkowski convolutional neural networks," in *Proceedings of the IEEE Conference on Computer Vision and Pattern Recognition*, 2019, pp. 3075–3084.
- [26] T. Le and Y. Duan, "Pointgrid: A deep network for 3d shape understanding," in *Proceedings of the IEEE Conference on Computer Vision and Pattern Recognition*, 2018, pp. 9204–9214.

- [27] H.-Y. Meng, L. Gao, Y.-K. Lai, and D. Manocha, "Vv-net: Voxel vae net with group convolutions for point cloud segmentation," in *Proceedings of the IEEE International Conference on Computer Vision*, 2019, pp. 8500–8508.
- [28] Z. Liu, H. Tang, Y. Lin, and S. Han, "Point-voxel cnn for efficient 3d deep learning," in *Advances in Neural Information Processing Systems*, 2019, pp. 965–975.
- [29] Q. Xu, X. Sun, C.-Y. Wu, P. Wang, and U. Neumann, "Grid-gcn for fast and scalable point cloud learning," in *Proceedings of the IEEE/CVF Conference on Computer Vision and Pattern Recognition*, 2020, pp. 5661–5670.
- [30] A. H. Lang, S. Vora, H. Caesar, L. Zhou, J. Yang, and O. Beijbom, "Pointpillars: Fast encoders for object detection from point clouds," in *Proceedings of the IEEE Conference on Computer Vision and Pattern Recognition*, 2019, pp. 12 697–12 705.
- [31] Z. Li, Y. Gan, X. Liang, Y. Yu, H. Cheng, and L. Lin, "Lstm-cf: Unifying context modeling and fusion with lstms for rgb-d scene labeling," in *European Conference on Computer Vision*. Springer, 2016, pp. 541–557.
- [32] S. Gupta, P. Arbeláez, R. Girshick, and J. Malik, "Indoor scene understanding with rgb-d images: Bottom-up segmentation, object detection and semantic segmentation," *International Journal of Computer Vision*, vol. 112, no. 2, pp. 133–149, 2015.
- [33] M. Tatarchenko, J. Park, V. Koltun, and Q.-Y. Zhou, "Tangent convolutions for dense prediction in 3d," in *Proceedings of the IEEE Conference on Computer Vision and Pattern Recognition*, 2018, pp. 3887–3896.
- [34] M. Simonovsky and N. Komodakis, "Dynamic edge-conditioned filters in convolutional neural networks on graphs," in *Proceedings of the IEEE Conference on Computer Vision and Pattern Recognition*, 2017, pp. 3693–3702.
- [35] Y. Li, R. Bu, M. Sun, W. Wu, X. Di, and B. Chen, "Pointcnn: Convolution on x-transformed points," in *Advances in Neural Information Processing Systems*, 2018, pp. 820–830.
- [36] J. Li, B. M. Chen, and G. Hee Lee, "So-net: Self-organizing network for point cloud analysis," in *Proceedings of the IEEE Conference on Computer Vision and Pattern Recognition*, 2018, pp. 9397–9406.
- [37] W. Wu, Z. Qi, and L. Fuxin, "Pointconv: Deep convolutional networks on 3d point clouds," in *Proceedings of the IEEE Conference on Computer Vision and Pattern Recognition*, 2019, pp. 9621–9630.
- [38] M. Atzmon, H. Maron, and Y. Lipman, "Point convolutional neural networks by extension operators," *arXiv preprint arXiv:1803.10091*, 2018.
- [39] M. Zhang, H. You, P. Kadam, S. Liu, and C.-C. J. Kuo, "Pointhop: An explainable machine learning method for point cloud classification," *IEEE Transactions on Multimedia*, 2020.
- [40] H. Lei, N. Akhtar, and A. Mian, "Spherical kernel for efficient graph convolution on 3d point clouds," *IEEE Transactions on Pattern Analysis and Machine Intelligence*, 2020.
- [41] Y. Liu, B. Fan, G. Meng, J. Lu, S. Xiang, and C. Pan, "Densepoint: Learning densely contextual representation for efficient point cloud processing," in *Proceedings of the IEEE International Conference on Computer Vision*, 2019, pp. 5239–5248.
- [42] A. Komarichev, Z. Zhong, and J. Hua, "A-cnn: Annularly convolutional neural networks on point clouds," in *Proceedings of the IEEE Conference on Computer Vision and Pattern Recognition*, 2019, pp. 7421–7430.
- [43] Y. Liu, B. Fan, S. Xiang, and C. Pan, "Relation-shape convolutional neural network for point cloud analysis," in *Proceedings of the IEEE Conference on Computer Vision and Pattern Recognition*, 2019, pp. 8895–8904.
- [44] S. Chen, C. Duan, Y. Yang, D. Li, C. Feng, and D. Tian, "Deep unsupervised learning of 3d point clouds via graph topology inference and filtering," *IEEE Transactions on Image Processing*, vol. 29, pp. 3183–3198, 2019.
- [45] Y. Rao, J. Lu, and J. Zhou, "Global-local bidirectional reasoning for unsupervised representation learning of 3d point clouds," in *Proceedings of the IEEE/CVF Conference on Computer Vision and Pattern Recognition*, 2020, pp. 5376–5385.
- [46] X. Gao, W. Hu, and G.-J. Qi, "Graphter: Unsupervised learning of graph transformation equivariant representations via auto-encoding node-wise transformations," in *Proceedings of the IEEE/CVF Conference on Computer Vision and Pattern Recognition*, 2020, pp. 7163–7172.
- [47] X. Xu and G. H. Lee, "Weakly supervised semantic point cloud segmentation: Towards 10x fewer labels," in *Proceedings of the IEEE/CVF Conference on Computer Vision and Pattern Recognition*, 2020, pp. 13 706–13 715.
- [48] N. Thomas, T. Smidt, S. Kearnes, L. Yang, L. Li, K. Kohlhoff, and P. Riley, "Tensor field networks: Rotation-and translation-equivariant neural networks for 3d point clouds," *arXiv preprint arXiv:1802.08219*, 2018.
- [49] C. Esteves, C. Allen-Blanchette, A. Makadia, and K. Daniilidis, "Learning so (3) equivariant representations with spherical cnns," in *Proceedings of the European Conference on Computer Vision (ECCV)*, 2018, pp. 52–68.
- [50] T. S. Cohen, M. Geiger, J. Köhler, and M. Welling, "Spherical cnns," *arXiv preprint arXiv:1801.10130*, 2018.
- [51] J. Yang, H. Li, D. Campbell, and Y. Jia, "Go-icp: A globally optimal solution to 3d icp point-set registration," *IEEE Transactions on Pattern Analysis and Machine Intelligence*, vol. 38, no. 11, pp. 2241–2254, 2015.
- [52] A. Myronenko and X. Song, "Point set registration: Coherent point drift," *IEEE Transactions on Pattern Analysis and Machine Intelligence*, vol. 32, no. 12, pp. 2262–2275, 2010.
- [53] M. A. Uy, Q.-H. Pham, B.-S. Hua, T. Nguyen, and S.-K. Yeung, "Revisiting point cloud classification: A new benchmark dataset and classification model on real-world data," in *Proceedings of the IEEE International Conference on Computer Vision*, 2019, pp. 1588–1597.
- [54] L. Yi, V. G. Kim, D. Ceylan, I.-C. Shen, M. Yan, H. Su, C. Lu, Q. Huang, A. Sheffer, and L. Guibas, "A scalable active framework for region annotation in 3d shape collections," *ACM Transactions on Graphics (TOG)*, vol. 35, no. 6, pp. 1–12, 2016.